ELSEVIER

Materials Science and Engineering A245 (1998) 168–181

MATERIALS SCIENCE & ENGINEERING A

Effects of morphology on the decohesion of compressed thin films

M.Y. He [a], A.G. Evans [b,*], J.W. Hutchinson [b]

[a] *Department of Materials, University of California, Santa Barbara, CA 93106, USA*
[b] *Division of Engineering and Applied Sciences, Harvard University, Cambridge, MA 02138, USA*

Abstract

Residually compressed thin films are susceptible to spalling from substrates. A prerequisite for this to occur is that a separation develop at the interface large enough to allow buckling. Thereafter, the mechanisms of spalling are well-established. In this article, the mechanics of formation of the initial separation are addressed. Perturbations on the interface are deemed responsible for this process. Calculations of energy release rates for various interface morphologies have revealed that aperiodic perturbations can initiate and extend the separations to a length sufficient for buckling. Conversely, periodic perturbations trap separations at dimensions too small to buckle. Illustrations are given for an alumina film (scale) on Ni-based superalloys. Implications for life prediction models are explored. © 1998 Elsevier Science S.A. All rights reserved.

Keywords: Thin films; Decohesion; Morphology

1. Introduction

Residually compressed thin films are susceptible to spalling from substrates [1–3]. When the film/substrate interface is well-bonded, failure occurs by thermomechanical fatigue, upon thermal cycling, caused by cyclic plasticity in the substrate near the interface [4]. However, a more debilitating problem arises when the interface adhesion is relatively low. Then, films typically decohere in accordance with the sequence indicated on Fig. 1 [1]. (i) A separation forms at the interface. (ii) Buckling occurs above the separation. (iii) The consequent energy release rate at the buckle perimeter causes it to propagate, often with a 'telephone cord' morphology. (iv) The interface crack kinks into the film and extends to the surface, resulting in dynamic spalling. In some cases (iii) and (iv) can be simultaneous. The mechanics of steps (ii) to (iv) are well-established [1–4]. The initial formation of the separation (step i) is not understood. The purpose of this article to explore phenomena that might induce initial separation.

Crack-like voids can form at interfaces upon oxidation. For this to occur remote from free edges, tensile or shear stresses must exist at the interface. For a planar interface these stresses are zero and there is no motivation for crack formation [5]. Consequently, nonplanarity has been proposed as a prerequisite for the growth of a separation large enough to case buckling [4]. One type of periodic interface undulation has been analyzed previously (Fig. 2, type I) [4]. Two others are examined in this study (Fig. 2, type II and III). The interface stresses induced by small periodic undulations can be expressed in the form:

$$\sigma_{ij}/\sigma_o = (A/L)Q_{ij}(\alpha_D, h/L) \quad (1a)$$

where σ_o is the compressive misfit stress in the film,

$$\sigma_o = E_1\epsilon^T/(1-\upsilon_1) \quad (1b)$$

with ϵ^T the misfit strain, E_1 the Young's modulus of the film and υ_1 its Poisson ratio. L is the wavelength of the undulations and A their amplitude, with h the film thickness. The function Q_{ij} depends on the first Dundurs' parameter, $\alpha_D = (\bar{E}_1 - \bar{E}_2)/(\bar{E}_1 + \bar{E}_2)$, where $\bar{E}$ is the plane strain modulus, with the subscripts 1 and 2 referring the film and substrate, respectively. It is insensitive to the second Dundurs' parameter [6]. Results for the shear stresses that arise with type I morphology [4] indicate magnitudes of Q from 1 to 4, depending on the elastic mismatch. Aperiodic features commonly present in films and scales, such as that indicated on Fig. 2d, create a stress environment that enhances the interface separation. Analysis of these perturbations constitutes a major objective of this article.

* Corresponding author. Harvard University, Pierce Hall 311, 29 Oxford Street, Cambridge, MA 02138 USA. Tel.: +1 617 4960424; fax: +1 617 4960601.

PII S0921-5093(97)00848-4

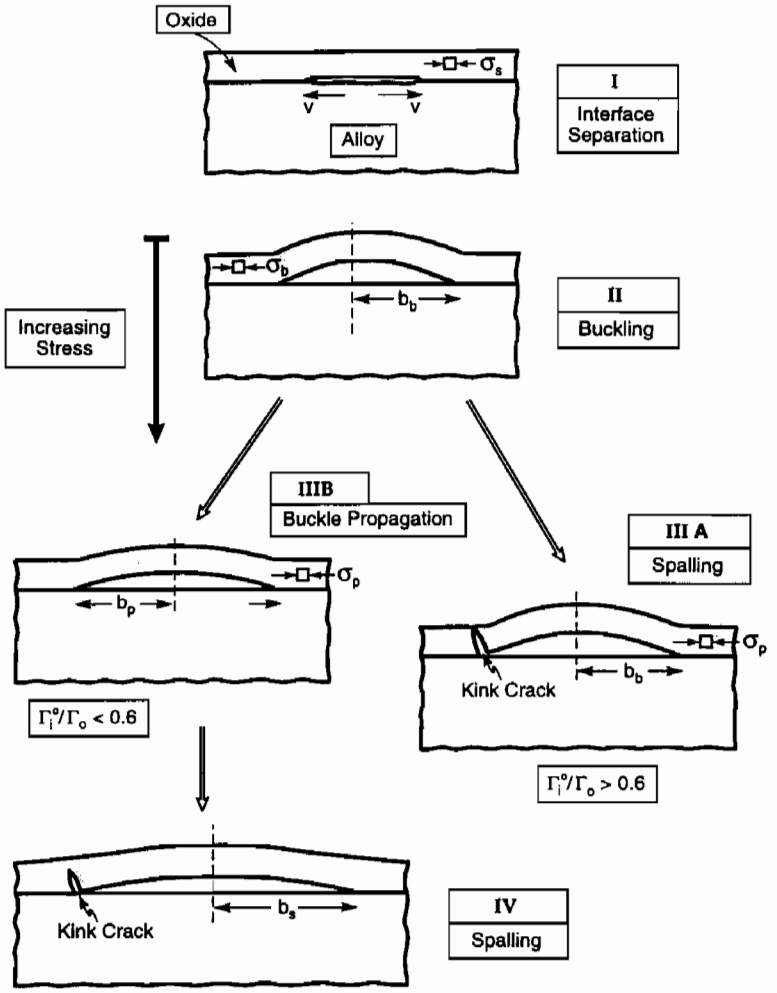

Fig. 1. The sequence of events that cause a thin compressed film to decohere from a substrate.

To address spalling, it is not sufficient to know the stresses. It is required that the behavior of interface separations be determined [1]. This is manifest as the energy release rate G relative to the adhesion. The principal objective of this study is to calculate G for interface separations that arise in conjunction with the morphologies indicated on Fig. 2 and, thereby, simulate crack growth along the interface.

To realize this objective, the article is organized in the following manner. (i) The mechanics of spalling (Section 2), establish the requirements. (ii) The stresses at the interface (Section 3) and the energy release rates for interface cracks (Section 4) determine the morphologies having the greatest potential for crack formation. (iii) Implications for the separation dynamics are explored in Section 5.

When illustrations of the mechanics are needed to assess their applicability, emphasis is given to the behavior of compressed Al_2O_3 thin films on Ni-based superalloys [7,8]. In particular, the oxide is considered to form by oxidation of Al in the alloy. It is subject to a moderate stress at high temperature, upon oxidation. However, on cooling, a large residual compression develops because of thermal expansion misfit. For these interfaces, segregation (particularly of S) is believed to adversely affect the adhesion [9–11].

2. Spall mechanics

Each of the events depicted in Fig. 1 involves a critical stress and a characteristic size [1–5]. Definition of these critical quantities provides a basis for experimental benchmarking and validation of the mechanisms.

(i) Buckling is explicitly defined. For films subject to biaxial compression, the critical separation radius, b_b, for axisymmetric buckling at stress, σ_b, is [1]:

$$b_b/h = 1.1\sqrt{E/\sigma_b} \quad (2a)$$

where E is the Young's modulus of the oxide and h its thickness. Thus, for a specified stress and film thickness, b_b represents the smallest separation radius that buckles. The analogous result in plane strain for a buckle of half width b_b is:

$$b_b/h = 0.9\sqrt{E/\sigma_b} \quad (2b)$$

(ii) Buckle propagation inherently involves mode mixity effects (Fig. 3) and associated changes in the interface toughness. Here, ψ is used to represent the mixity angle with 0 referring to mode I and $\pm\pi/2$ to mode II. For a typical case, wherein the interfaces exhibit higher mode II than mode I toughness, there is a 'critical' stress, σ_p above which buckles always propagate. This stress is given for axisymmetric buckles by [1]:

$$\sigma_p = \phi\sqrt{E\Gamma_i^o/(1-\upsilon)h} \quad (3)$$

where υ is Poisson's ratio, Γ_i^o the mode I interface toughness and ϕ about 2.5. There is a corresponding 'critical' size, b_p, below which buckles should not propagate. This size is:

$$b_p/h = \omega\sqrt{E/\sigma_p} \quad (4)$$

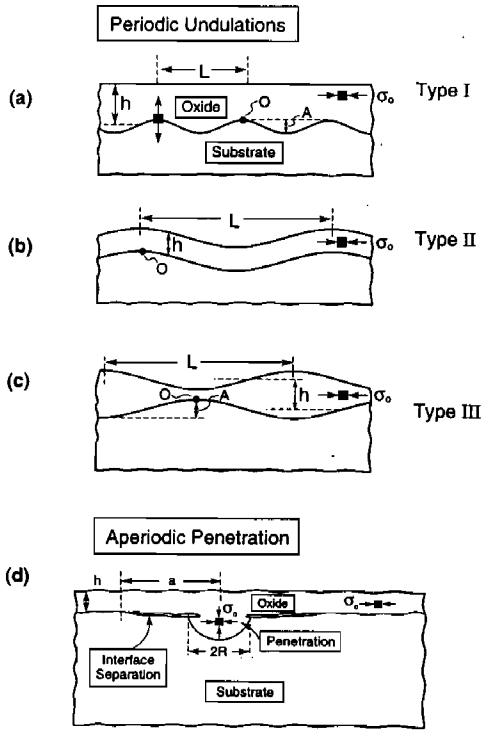

Fig. 2. The four film morphologies addressed in the present analysis.

where $\omega \approx 2$. Note that b_p is about twice that for buckling, b_b (Eq. (2a)), at comparable stress levels and film thicknesses.

(iii) The deflection of the interface crack into the film occurs in accordance with a kinking criterion [1,12]. This criterion is dictated by the mode mixity and the ratio of the interface toughness, Γ_i^o, to that for the film, Γ_o. Graphical representation (Fig. 3a,b) reveals that spalling, rather than continued propagation along the interface, happens when the interface is relatively tough: $\Gamma_i^o/\Gamma_o \gtrsim 0.56$. Then, the spall size is the same as the buckle size: $b_s = b_b$ (Eq. (2a)). The stress at which the spall occurs, σ_s has the form;

$$\sigma_s = \phi^*\sqrt{E\Gamma_o/(1-\upsilon)h} \quad (5)$$

with $\phi^* \sim 1.7$. However, at smaller interface toughnesses, the buckle propagates along the interface (at stress σ_p) before it spalls. The actual spalling event is then critically dependent upon mode mixity details [1]. Specifically, since the magnitude of the mixity angle increases as the buckle extends (Fig. 3c), there is a greater tendency for kinking at larger buckles (Fig. 3d). The spall size, b_s (Fig. 3a–d) is:

$$b_s/h = \chi\sqrt{E/\sigma_p} \quad (6)$$

where χ is estimated from [1] as:

$$\chi \approx 1.1\exp[0.7(\Gamma_o/\Gamma_i^o) - 1.25] \quad (7)$$

This result applies for rough interfaces wherein the mode II interface toughness exceeds that for mode I by about an order of magnitude [5,13,14]. Note that the spall radius can be extremely large when the interface toughness is small.

Application of these mechanics is illustrated for oxide scales, thickness $h = 1$ μm, on Ni alloys ($E_1 = 400$ GPa, $E_2 = 200$ GPa). Two estimates for the interface fracture energy have been used. One is the value (10 J m^{-2}) measured for diffusion bonded Ni/alumina interfaces at room temperature [15,16]. The other (1 J m^{-2}) is an estimate for an interface with diminished toughness caused by segregation [17,18]. The corresponding film toughness is: $\Gamma_o \approx 20$ J m^{-2}. The critical stresses found from Eqs. (3) and (5) are, $\sigma_o = 2$–6 GPa, for both buckle propagation and spalling: the smaller stress referring to the lower interface toughness. These bound the thermal expansion misfit stress for this material system: ~3.5 GPa [7,8,19]. Consistency thus exists, but is contingent on segregation to diminish the interface toughness to about 1 J m^{-2}. The critical radii for buckle propagation (Eq. (4)) range from 16 to 27 μm. The corresponding spall sizes (Eq. (6)) vary from 16 μm to 3 mm. These are in the range reported in the literature [9,20], but the comparison is not discriminating.

Most importantly, for buckling to occur, separations of order 20 μm must exist at the interface. An under-

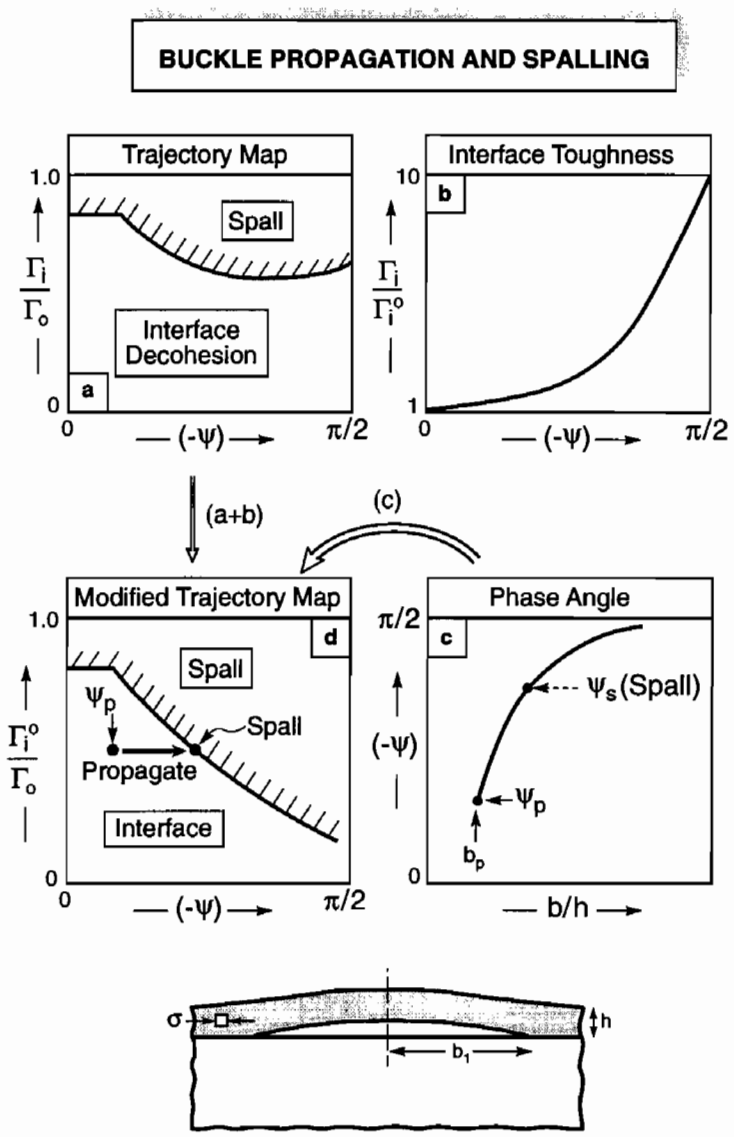

Fig. 3. Mode mixity effects and their role in determining the incidence of spalling.

standing of the initial formation of such separations is essential to a self-consistent mechanistic model. The separations may either form at high temperature, facilitated by diffusive crack growth mechanisms [21], or may develop as the stress builds up on cooling. These are discussed in some detail in Section 5. Here, it is noted that interface separation is characterized by a threshold condition, dictated by the work of adhesion, W_{ad}, below which they are unable to propagate. That is, the effective interface toughness at high temperature is $\Gamma_i \approx W_{ad}$. Consequently, by calculating G_1 and equating to W_{ad}, the likelihood of growing separations up to the magnitude needed for buckling, upon subsequent cooling, will be determined.

3. Stresses

3.1. Periodic morphology

The stresses associated with the periodic morphologies in Fig. 2 can be calculated analytically for the case of small undulation amplitudes ($A/L < 0.2$ and $A/h < 0.2$). The coordinates (x_1, x_2) are defined on Fig. 4a. The analysis is performed using the perturbation approach described elsewhere [4]. The stresses at any point in the substrate or along the interface can be expressed in accordance with (Eq. (1a)). Emphasis in [4] was placed on the effective von Mises stress in the substrate, which was found to be nearly independent of x_1 just below the interface. Normal stresses occur at the

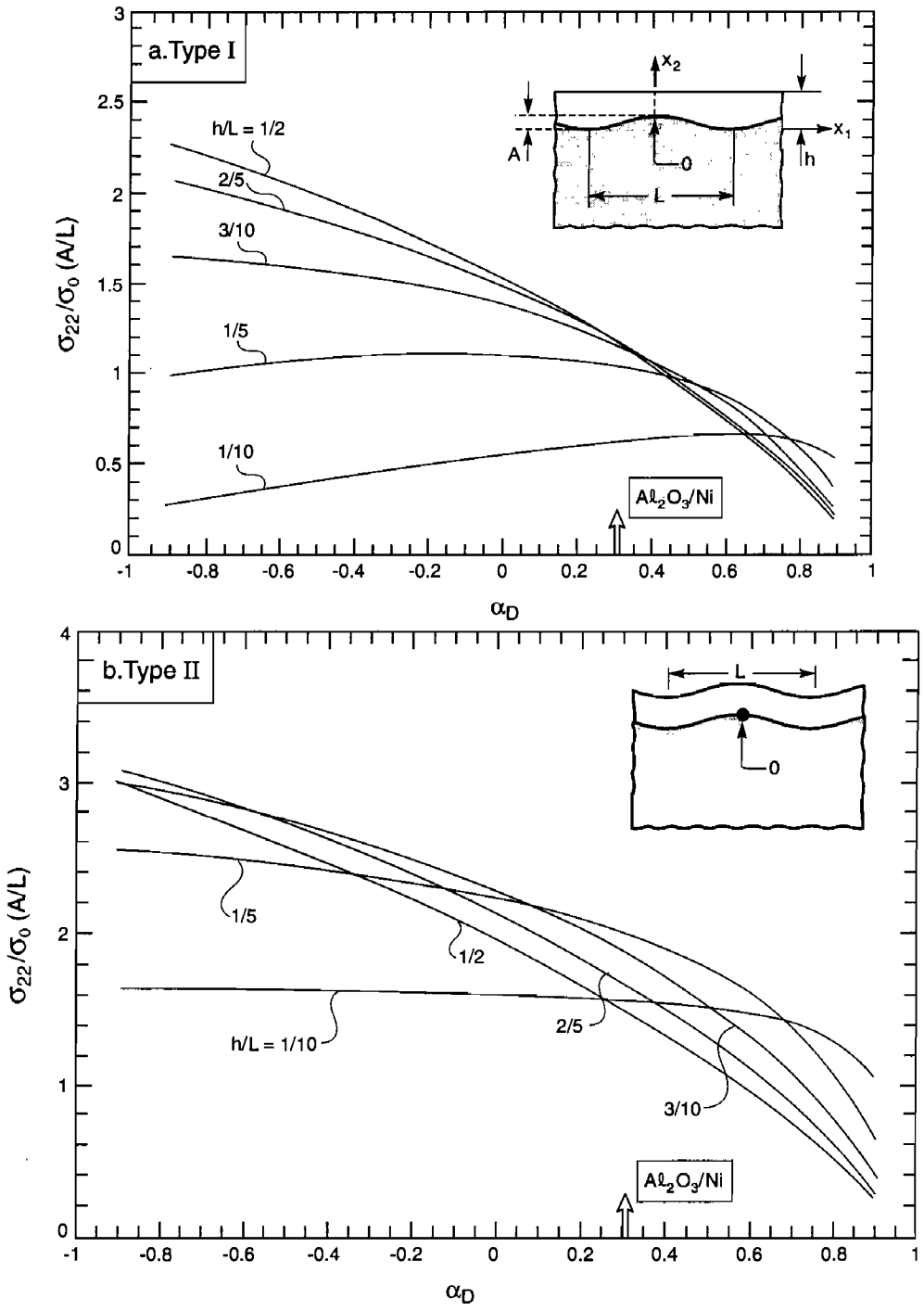

Fig. 4. Normal stresses at the concave sites along the interface calculated for the three periodic morphologies.

peaks and valleys along the interface, while shear stress occurs halfway between the peaks and valleys. In this paper, emphasis centers on normal stresses acting at the interface and their tendency to foster interface fracture. When the film is in compression, a tension acts across the interface at the undulation peaks, except for long wavelength undulations of type III. Plots of the amplitude-modified stress parameter (Q_{22}) acting across the interface at the peaks are presented in Fig. 4, as a function of the first Dundurs' parameter, for each of

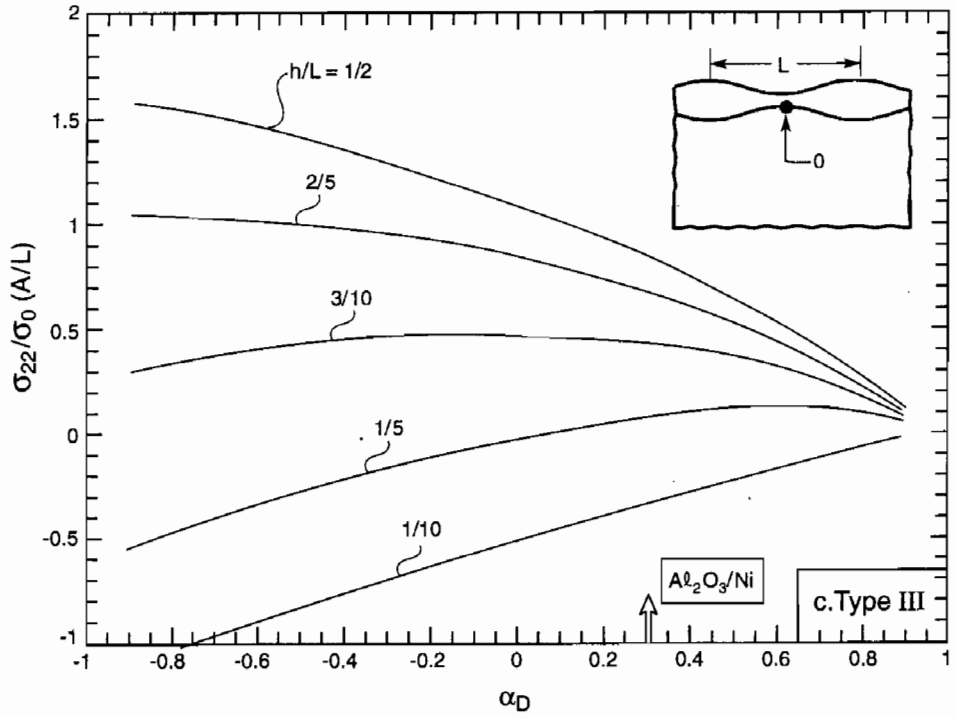

Fig. 4. (*Continued*)

the three types of undulation. (In [4], σ_o was defined to be positive in tension. Here it is taken to be positive in compression such that, on Fig. 4, the positive σ_{22} stresses are tensile). Even relatively small undulations produce significant interface stresses when σ_o is large. For elastic properties relevant to the Al_2O_3 interface ($\alpha_D \approx 0.3$), the stress parameter Q_{22}, is in the range 0.5–2.0 for most wavelengths of practical interest ($1/5 \leq h/L \leq 1/2$. The shear stress on the interface at points halfway between the peaks and valleys are of comparable magnitude to the normal stress and display less dependence on h/L (see [4] for type I). For type III undulations, at long wavelengths ($h/L \leq 1/5$), the location of the maximum tensile interface stress shifts to the valleys.

3.2. Aperiodic morphology

The elastic stresses that develop around aperiodic penetrations are calculated numerically, with emphasis on the equivalent values, σ_e. The stress contours are shown on Fig. 5, normalized by σ_o defined above. Note that the maximum equivalent stresses near the interfaces are $\sigma_e/\sigma_o \approx 0.35$. In practice, these stresses cause yielding when σ_e reaches the tensile yield strength of the substrate, σ_y. Consequently, the stress in the penetration is limited to $\sim 2.8\sigma_y$. (A full elastic/plastic calculation would be needed to establish the exact magnitude of this stress ratio). There is no corresponding effect in the remainder of the film, because it does not generate a large stress in the substrate, except locally near the periodic oscillations.

This stress relaxation is important when assessing the potential for penetrations to induce interface separations. Substrate (bond coat) yielding must be included as a factor that limits the stress in the penetration. That is, all other factors being equal, lower yield strength bond coats diminish the importance of penetrations for separation and spalling.

4. Energy release rates

4.1. Periodic morphologies

By introducing small cracks at the interface, energy release rates, G, are calculated. For periodic morphologies (Fig. 2a–c), plane strain cracks are considered that originate in a region of interface tension and spread symmetrically along the interface (Fig. 6). Dimensional analysis indicates that

$$\bar{E}_1 G/\sigma_0^2 A = \omega(\alpha_D, a/L, A/h, h/L) \tag{8a}$$

where $2a$ is the crack length and ω is the function to be calculated. There is also a weak dependence on the second Dundurs' mismatch parameter, which has not been recorded. Illustrative results are presented on Fig. 6 (for $\alpha_D \approx 0.3$, relevant to the Al_2O_3/Ni interface).

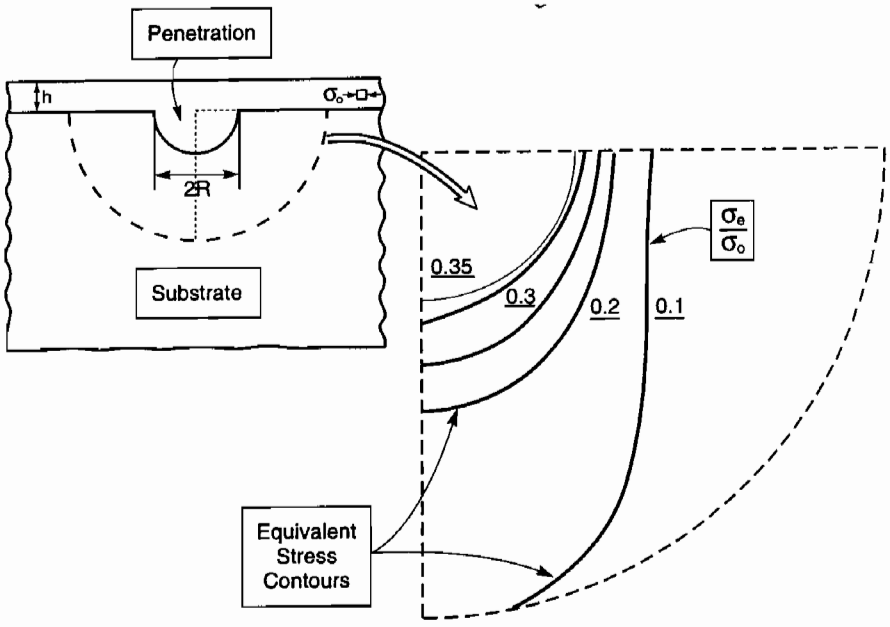

Fig. 5. Elastic equivalent stress contours associated with a hemispherical penetration.

These results and others for the aperiodic morphologies (Figs. 8–12), were calculated by the virtual crack extension method using the ABAQUS code. It has been found that G oscillates with a period governed by L (exemplified in Fig. 6a for a type III morphology), reaching nearly zero when the tip is about halfway between the valley and the next peak. Fig. 6b emphasizes growth out into the first valley. Such growth is relatively insensitive to the morphology for typical wavelengths and amplitudes: $h/L = 0.3$, $A/L = 0.2$. More generally, because of the differences in stress among the three morphologies (Fig. 4), energy release rate distinctions are expected to arise. These are not addressed in the present study.

The quasi-steady-state behavior seen in Fig. 6a for cracks longer than about $2L$ arises because the interface stresses within each undulation are released upon separating the film. The associated energy released is nominally available for crack extension. The perturbation method of [4] can be applied to determine the energy release rate for long cracks averaged over a wavelength L, denoted by $(G_{ss})_{ave}$. The method evaluates the difference in elastic energy between the bonded and debonded geometries. (It is important to note that the coating remains attached to the substrate on each end of the crack. The average strain in the film parallel to the interface is not altered by debonding). The result of the analysis for the type I morphology is shown in Fig. 7. These results are accurate for small undulations (i.e. $A/L < 0.2$ and $A/h < 0.2$). The limit for long wavelengths ($h/L \ll 1$) is independent of the elastic mismatch between the film and substrate and is the same for morphologies I and III:

$$(G_{ss})_{ave} = \frac{\sigma_o^2 h}{4\bar{E}_1}\left(\frac{A}{h}\right)^2 \tag{8b}$$

The factor $(1/2)\sigma_0^2 h/\bar{E}_1$ is the well-known plane strain expression for the energy release of a delamination crack on a planar interface, wherein one end of the film has detached from the substrate and all the elastic energy in the film is released [1]. Note that, since $A \ll h$, $(G_{ss})_{ave} \to 0$ as $h \to 0$ and as $A \to 0$. This gives some perspective on the average energy release rate for relatively small interface undulations. However, it is essential to realise that the energy release rate oscillates about this average, with crucial consequences for the stability of small separations, elaborated next.

4.2. Aperiodic penetrations

The results for the periodic morphologies in Fig. 6a (which are inclusive of crack interactions), imply that separations are trapped in the vicinity where G becomes very small. They cannot extend by more than one wavelength before they arrest. Such separations are too small to enable buckling. Solutions for aperiodic (local) penetrations indicate greater potential for the growth of separations. They reveal that finite energy release rates persist to appreciable crack extensions relative to the film thickness (Fig. 8). This morphology induces energy release rates in accordance with other, comparable dilatational phenomena. These other phenomena include: lateral cracking from hardness indentations [22], microcracking from transforming particles [23] and cracking from inclusions caused by thermal expansion mismatch [24]. From these previous analyses, the non-dimensional

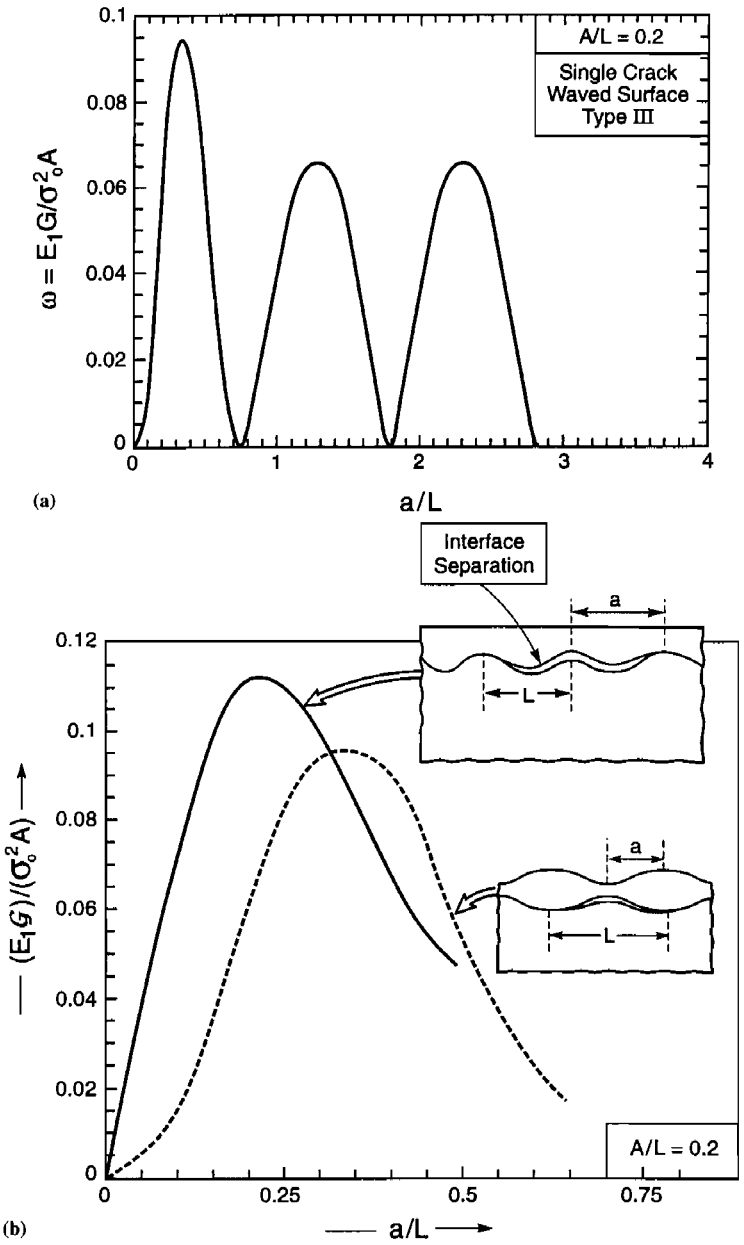

Fig. 6. Non-dimensional plane strain energy release rates for periodic morphologies: (a) effect of crack length for the in-phase periodic morphology, (b) small cracks comparing two morphologies.

energy release rate is known to be strongly dependent on the assumption made about the location of the inner crack front [23,24]. Typically, this front extends toward the center of symmetry, either along the interface or partially through the penetration. To bound the behavior, solutions are obtained by: (a) allowing the inner front to be trapped at the interface and (b) letting the energy release rate at this crack front be zero. In many cases, the separation dynamics are dominated by the opening (mode I) energy release rate, G_I, because the shear (mode II) does not contribute to the separation mechanism [21]. Mode mixity angles ψ are thus explored. Among a range of results presented on Figs. 8–12, the predominant features are as follows.

(i) There is a substantial effect of the condition imposed at the inner crack front (Fig. 9a), especially when the interface crack is small. Cracks that extend inward have considerably larger energy release rates at

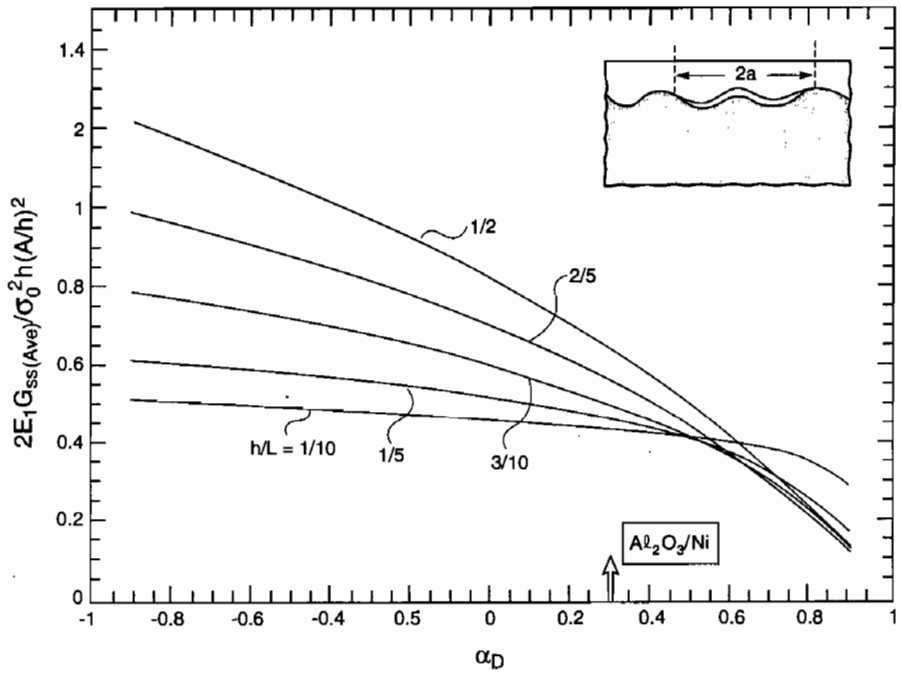

Fig. 7. The quasi steady-state energy release rate for cracks that form in association with type I periodic morphology.

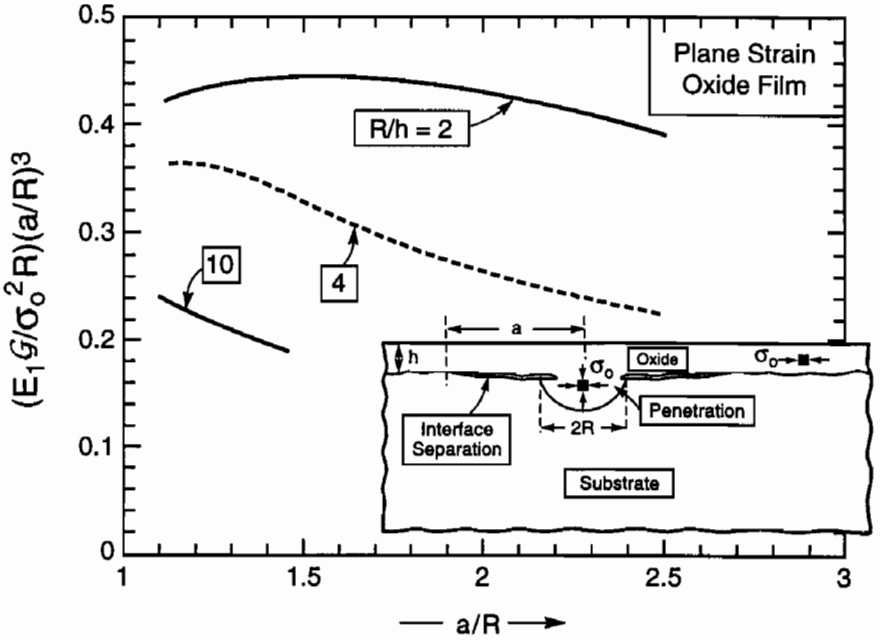

Fig. 8. Plane strain energy release rates for the aperiodic penetration with the inner crack at zero energy release rate.

the outer edge. The rate at which G builds up as the inner crack front penetrates the particle is indicated on Fig. 9b for axisymmetric penetrations. Evidently, penetrations about half way into the particle are sufficient to develop the full energy release. The trend is the same in plane strain. For further analysis, the solutions with zero G at the inner crack front are used.

(ii) The energy release rates attained with planar penetrations (Fig. 8) are substantially larger than those for hemispherical penetrations (Fig. 10).

(iii) Non-dimensional energy release rates, E_1G/σ_o^2h, decrease as the crack extends. Moreover, plane strain penetrations (Fig. 8), when the normalization is changed such that R is replaced by h, the following approximation characterizes the energy release rate:

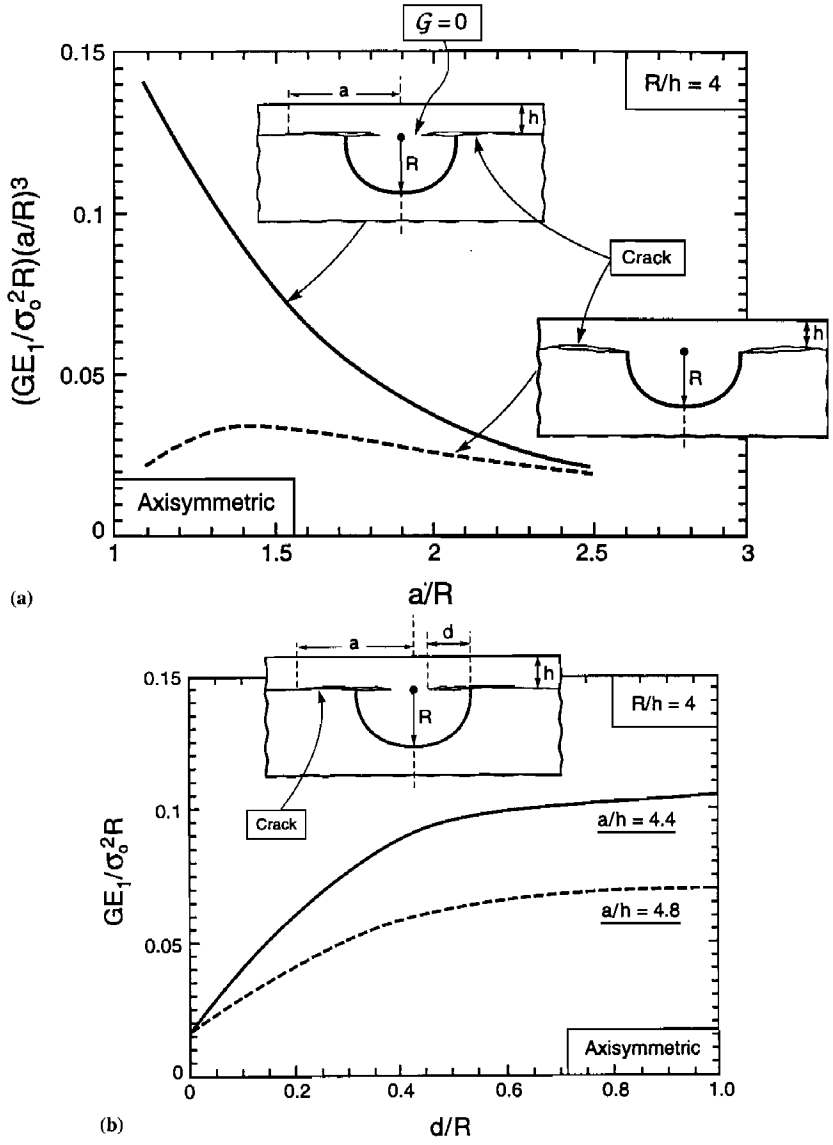

Fig. 9. (a) The effects of the condition imposed at the inner crack front on the energy release rate for an axisymmetric penetration. (b) The change in energy release rate as the inner crack front is allowed to progress through the penetration.

$$\frac{E_1 G}{\sigma_o^2 h} \approx \left(\frac{R}{a}\right)^3 \tag{9}$$

(iv) An overlay coating changes the behavior. The effect is illustrated (Fig. 11) for a thick coating having properties characteristics of a porous ZrO_2 thermal barrier (modulus, $E = 100$ GPa, and thermal expansion coefficient, $\alpha = 10^{-5}\ C^{-1}$). For small separations, the energy release rate is lower than that for the film only, presumably governed by the extra stiffness provided by the coating. But, at longer separations some of the residual energy density in the coating becomes available for crack growth and G becomes relatively larger.

(v) The mode mixity angle in the absence of an overlay coating is essentially constant, with $\psi = 80°$ (Fig. 12). That is, the debond is predominantly mode II. However, when an overlay is superposed, ψ decreases as the debond extends, rendering it more susceptible to propagation. These mixity characteristics are not explicitly used in the subsequent analysis. But they will need to be included in a full treatment of interface cracking and spalling, because of the strong effect of ψ on the interface fracture toughness.

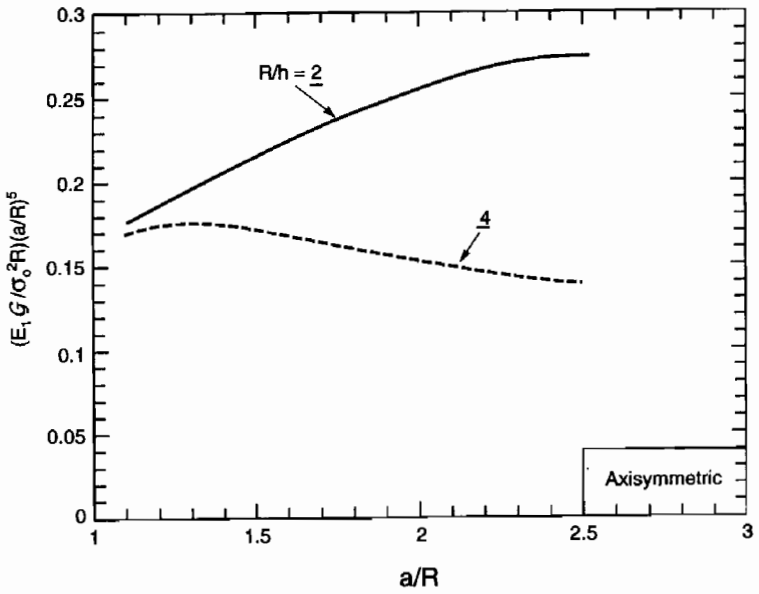

Fig. 10. Energy release rates for axisymmetric penetrations.

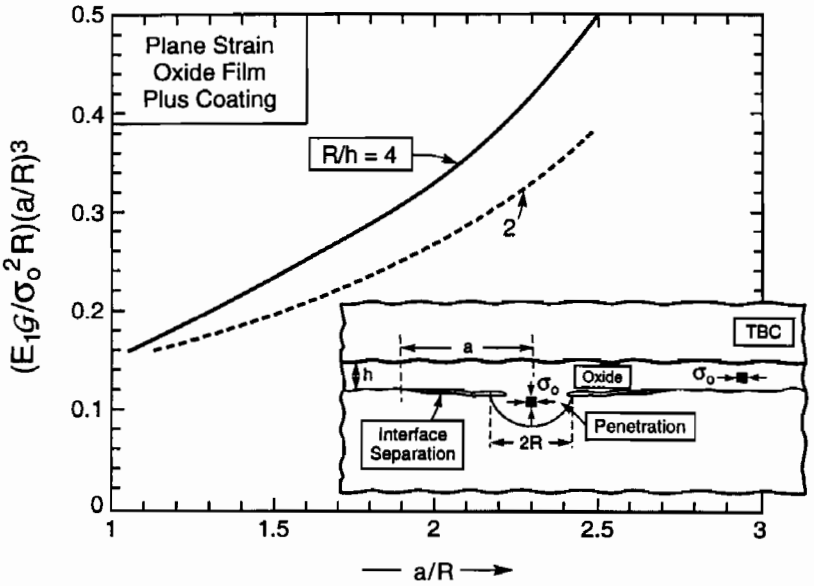

Fig. 11. Effect of a thick overlay coating having properties typical of porous ZrO_2 on the plane strain energy release rates for an interface separation.

5. Implications for life prediction

5.1. Buckling

It is instructive to assess the effectiveness of penetrations as a source of separations large enough to cause buckling. This is achieved by combining Eq. (9) with Eq. (2a) and equating G to Γ_i to give a critical penetration radius, R_c. If the misfit stress in the film and the penetration are both σ_o, the result is:

$$R_c/h = 0.9(E_1/\sigma_o)^{5/6}(\Gamma_i/\sigma_o h)^{1/3} \quad (10)$$

A plot of R_c/h against σ_o/E_1 for a range of $\sigma_o h/\Gamma_i$ (Fig. 13) provides a map of the penetration size domain that enables buckling. (Recall Γ_i that refers to a mode mixity angle, $\psi = 80°$). To be explicit, choosing parameters relevant to thermally grown Al_2O_3 on Ni(Al) alloy ($\sigma_o \approx 3$ GPa, h ≈ 1 μm, $E \approx 400$ GPa) and if $\Gamma_i \approx 1$ J m^{-2}, then the critical size is: $R_c \approx 3$ μm. However, if the stress is only $\sigma_o \approx 1$ GPa, then R_c increases to ~ 10 μm.

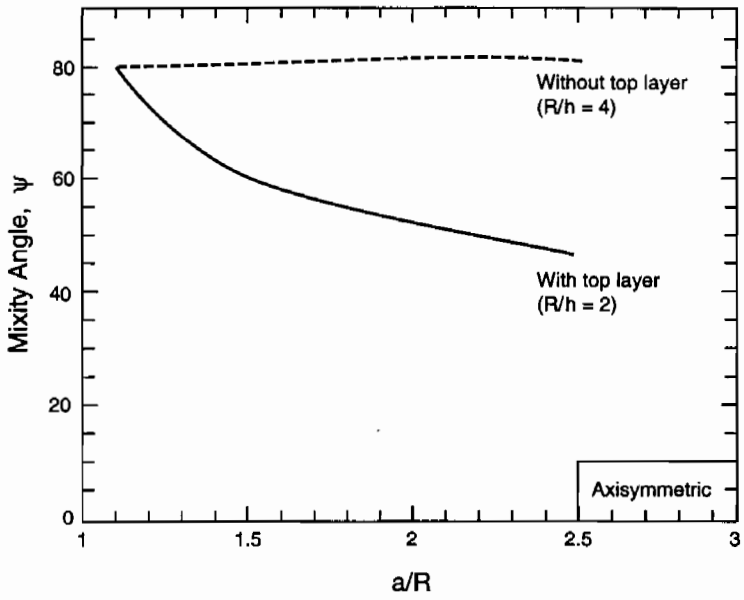

Fig. 12. Mode mixities as a function of crack length for axisymmetric penetrations with and without an overlay coating.

5.2. Separation dynamics

The energy release rates and the stresses can be used to predict some effects that occur in compressed thin films. One response is addressed: the steady growth of cracks at oxide scale/superalloy interfaces occurring at high temperature. Effects of thermal cycling with an adherent film have been addressed elsewhere [4].

For this illustration, two phenomena are involved. (i) A dwell at high temperature that enables interface separations to form as a consequence of growth stresses. That is, compressive growth stresses in the oxide, σ_g, that couple into the interface through the undulations, provide an energy release rate in accordance with Eq. (9), upon replacing σ_o with σ_g. (ii) This dwell process results in a separation having length, $2b$. The dwell is followed by a cooling period wherein the stresses elevate because of the thermal expansion misfit. For spalling to occur, the separation that forms in the dwell must be large enough to satisfy the buckling condition upon subsequent cooling to room temperature, in accordance with Eq. (2a).

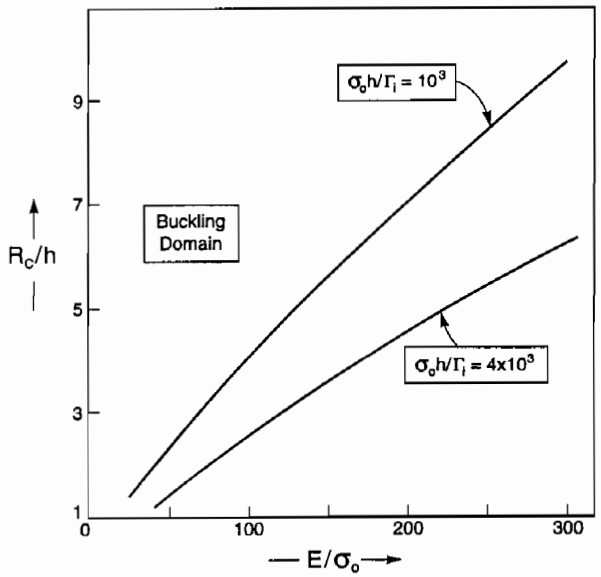

Fig. 13. A buckling map determined for separations growing from aperiodic linear penetrations. Buckling is possible in the top left domain.

It is assumed that crack-like void growth at the interface is the mechanism of separation. This happens whenever the energy release rate exceeds the work of adhesion W_{ad}, [21]. The underlying phenomena are vividly illustrated in recent experimental observations made for NiO films grown on a Ni-based alloy (unpublished research). The mathematical statements that represent this behavior are as follows.

(i) The separation that forms in the dwell period must satisfy the propagation and spall conditions Eq. (6):

$$a \geq b_s \tag{11a}$$

(ii) The stress at room temperature must exceed that needed to propagate the interface crack up to the spall size:

$$E_1(\Delta\alpha\Delta T + \epsilon_\infty)/(1-\upsilon) + \sigma_g \geq \sigma_s \tag{11b}$$

where σ_g is the stress operating at high temperature and ϵ_∞ the applied strain (which introduces a thermome-

chanical fatigue element). Assessment of the inequality (Eq. (11b)), using Eq. (3), establishes a minimum film thickness that has to be generated in the dwell period. This thickness is:

$$h \geq \frac{(\Gamma_i/E_1)\phi^2(1-\upsilon)}{[\Delta\alpha\Delta T+\epsilon_*]^2} \tag{12a}$$

where $\epsilon_* \equiv \epsilon_\infty + \epsilon_g$ [with $\epsilon_g \equiv \sigma_g(1-\upsilon)/E_1$]. Simultaneous satisfaction of the inequality (Eq. (11a)) along with Eq. (6) requires that:

$$a \geq \frac{2h}{[\Delta\alpha\Delta T+\epsilon_*]^{1/2}} \tag{12b}$$

Combining these requirements with the separation size gives an expression that depends on the dwell time t_d.

If plane strain penetrations dominate the energy release rate, then upon equating G to W_{ad}, Eq. (9) together with Eq. (12a) gives:

$$R \geq 2\left(\frac{\phi^2(1-\upsilon)\Gamma_i}{\sigma_g}\right)^{2/3} \frac{(W_{ad}/E_1)^{1/3}}{[\Delta\alpha\Delta T+\epsilon_*]^{11/6}} \tag{13}$$

where R is dependent on the dwell t_d. The diffusion-controlled growth of penetrations has the general form [25],

$$R = \sqrt{2c_x D_x t_d} \tag{14}$$

where D_x is a diffusivity ($D_x \equiv D_o \exp[-Q_D/kT]$, with Q_D being the activation energy and k the Boltzmann constant) and c_x the supersaturation of the species x that forms the penetration. This species would typically be either an alloying element or an impurity (such as S). Combining Eq. (14) with Eq. (13), the dwell time needed to form a separation large enough to buckle and spall becomes:

$$t_d^* = 2\left(\frac{\phi^2(1-\upsilon)\Gamma_i}{\sigma_g}\right)^{4/3} \left[\frac{\exp[Q_D/kT]/(W_{ad}/E_1)^{2/3}}{D_o c_x[\Delta\alpha\Delta T+\epsilon_*]^{11/3}}\right] \tag{15}$$

This is the expression for the life when high temperature interface separation kinetics control spalling. All of the parameters in Eq. (15) can be independently measured in order to test the hypothesis. It is already apparent that Eq. (15) embraces the principal variables used in the engineering models [26,27]: namely $\Delta\alpha$, ΔT, T and Q_D.

More generally, interface growth instabilities occurring upon oxidation involve factors other than diffusion in the substrate [28]. A comprehensive model would require that all of these factors be addressed.

6. Concluding remarks

Interface morphology has been identified as a key feature in the formation of the initial separations that lead to buckling and spalling of compressed films. Most noteworthy is the distinction between isolated, aperiodic penetrations and periodic undulations. The former can motivate interface separations that extend over lengths many times the film thickness. Conversely, the latter provide oscillatory energy release rates that cause separations to be locally trapped. A direct implication is that small artificially created periodic perturbations along the surface would prevent interface debonds from coalescing and enhance film durability. However, such trapped separations would 'weaken' the interface and make it susceptible to removal upon mechanical loading.

When aperiodic penetrations are present, their ability to grow interface separations large enough to permit buckling, is strongly affected by their size, the stress and the interface toughness, in accordance with Eq. (11a). For misfit stresses in the 3 GPa range, typical of the thermal expansion misfit between oxides and metals ($\Delta\alpha \approx 5 \times 10^{-6}$ C^{-1}), and with high yield strength substrates, ($\sigma_y \geq 1$ GPa) critically-sized penetrations are about 3 μm, for a 1-μm thick film. These are in the size range recorded for typical oxide scales [6,7,9,19,29]. However, quite low interface toughnesses are still needed to enable spalling, about $\Gamma_i \approx 1$ J m^{-2} at mixity angles of order 80°. Such toughnesses are considerably lower than those found for diffusion bonded Ni/Al_2O_3 interfaces. But, segregation (e.g. of S) could reduce Γ_i to these levels [9,10]. Further understanding of such interface phenomena is needed before the role of penetrations can be validated.

In practice, aperiodic penetrations arise at grain boundaries in the substrate [6,7,19] and at chemical heterogeneities [9,29] that lead to locally enhanced oxide formation. The former are linear and provide the larger energy release rates for high temperature separation, accounting for their evident role in spall formation. The latter appear to be important in some cases, presumably dependent on segregation levels and the spatial extent of the heterogeneity. Additional studies of these perturbations would be needed to clarify their origin and magnitude.

Some preliminary analysis has been performed for an overlay, such as a thermal barrier coating (TBC). These provide background but further analysis is necessary. The TBC has been found to enhance the growth of separations (except when they are very small), because some of the energy density in the TBC is available for interface cracking. Moreover, the TBC increases the relative mode I contribution to the energy release rate primarily responsible for the high temperature growth of separations. Conversely, the TBC suppresses buckling and requires that larger separations form before spalling can occur.

References

[1] J.W. Hutchinson, Z. Suo, Adv. Appl. Mech. 29 (1992) 63–191.
[2] J.W. Hutchinson, M.D. Thouless, E.G. Liniger, Acta Metall. Mater. 40 (1992) 295–308.
[3] M.D. Thouless, H.M. Jensen, E.G. Liniger, Proc. R. Soc. Lond. A447 (1994) 271–279.
[4] A.G. Evans, M.Y. He, J.W. Hutchinson, Acta Mater. 45 (1997) 3543–3554.
[5] A.G. Evans, J.W. Hutchinson, Acta Metall. Mater. 43 (1995) 2507–2530.
[6] J. Dundurs, J. Appl. Mech. 36 (1969) 650–652.
[7] R.J. Christensen, D.M. Lipkin, D.R. Clarke, Acta Mater. 44 (9) (1996) 3813–3821.
[8] R.J. Christensen, V.K. Tolpygo, D.R. Clarke, Acta Mater. 45 (4) (1997) 1761–1766.
[9] J.L. Smialek, D.T. Jayne, J.C. Schaeffer, W.H. Murphy, Thin Solid Films 253 (1994) 285–292.
[10] J.G. Smeggil, Mater. Sci. Eng. 87 (1987) 261–265.
[11] B.A. Pint, A.J. Garratt-Reed, L.W. Hobbs, Mat. High Temps. 13 (1) (1995) 3–15.
[12] M.Y. He, J.W. Hutchinson, J. Appl. Mech. 56 (1989) 270–278.
[13] H.C. Cao, A.G. Evans, Mech. Mater. 7 (1989) 295–305.
[14] K.M. Liechti, Y.S. Chai, J. Appl. Mech. 59 (1992) 295.
[15] F. Gaudette, S. Suresh, A.G. Evans, G. Dehm, M. Rühle, Acta Mater. (in press).
[16] M.Y. He, J.W. Hutchinson, J. Appl. Mech. 56 (1989) 270–278.
[17] A. Bagchi, A.G. Evans, Interface Sci. 3 (1996) 1.
[18] D. Lipkin, PhD thesis, Materials, UCSB, 1996.
[19] D.M. Lipkin, D.R. Clarke, Oxid. Metals 45 (3/4) (1996) 267–280.
[20] P.Y. Hou, J. Stringer, Oxid. Met. 38 (1992) 323–345.
[21] T. Chuang, J.-L. Chu, S. Lee, Trans. ASME 63 (1996) 796.
[22] B.R. Lawn, A.G. Evans, J. Mater. Sci. 12 (1977) 2195.
[23] M. Rühle, A.G. Evans, R.M. McMeeking, P.G. Charalambides, J.W. Hutchinson, Acta Metall. 35 (1987) 2701–2710.
[24] D.K.M. Shum, Y.Y. Huang, Eng. Fracture Mech. 37 (1990) 107–117.
[25] J.S. Kirkaldy, D.J. Young, Diffusion in the Condensed State, Inst. Metals, London, 1987.
[26] T.A. Cruse, S.E. Stewart, M. Ortiz, J. Eng. Gas Turbines Power 110 (1988) 610–616.
[27] S.M. Meier, D.M. Nissely, K.D. Scheffler, Final Report NASA CR-189111, 1991.
[28] H. Schmalzreid, Chemical Kinetics of Solids, VCH Verlagsgesellschaft, Weinheim, 1995.
[29] E. Schumann, J.C. Yang, M.J. Graham, M. Rühle, Mater. Corrosion 46 (1995) 218–222.